Postbuckling Behavior of Selected Curved Stiffened Graphite-Epoxy Panels Loaded in Axial Compression

Norman F. Knight Jr.* and James H. Starnes Jr.†
NASA Langley Research Center, Hampton, Virginia

Results of an experimental and analytical study of the postbuckling behavior of selected curved stiffened graphite-epoxy panels loaded in axial compression are presented. The postbuckling response and failure characteristics of the panels are described. Each panel had four equally spaced I-shaped stiffeners and 16 ply quasi-isotropic skins. Panels with three different stiffener spacings were tested. Failure of all panels initiated in a skinstiffener interface region. Analytical results from a nonlinear general shell finite-element analysis computer code correlate well with typical postbuckling test results up to failure. The analytical modeling detail necessary to predict accurately the response of the panel is described. Measured initial geometric imperfections were included in the postbuckling analysis. Typical stress distributions in the skinstiffener interface region were determined analytically.

Nomenclature

b = stiffener spacing
$\bar{b}$ = width of uniform-thickness flange
C = panel chord length
e = strain
e_{cr} = longitudinal strain at buckling
EA = prebuckling extensional stiffness
$\bar{h}$ = height of uniform-thickness flange
L = panel length
P = applied load
P_{cr} = analytical buckling load
P_{fail} = applied load at failure
R = panel radius of curvature
t = panel skin thickness
u = end shortening
u_{cr} = end shortening at buckling
u_{fail} = end shortening at failure
w = out-of-plane displacement
$w_{\max}$ = maximum w used to normalize the contour plots in Fig. 11 for each indicated value
$w_0(x, y)$ = initial geometric imperfection
$(w_0)_{\max}$ = maximum value of $w_0(x,y)$
$(w_0)_{\text{mean}}$ = mean value of $w_0(x,y)$
$(w_0)_{\text{rms}}$ = standard deviation of $w_0(x,y)$
W = panel arc length or width
x, y = surface coordinates
ξ_{mn} = mean imperfection amplitudes

Introduction

CURRENT metal aircraft design practice allows the skin panels of some structural components (e.g., fuselage and stabilizer panels) to buckle under various loading conditions and are designed to have postbuckling strength. Before advanced composite structural components can be designed with similar postbuckling response, their strength limits and failure characteristics must be well understood. Most previous work on the postbuckling behavior of compression-loaded composite structures (e.g., Refs. 1–4) has focused on analytical solutions to classical unstiffened orthotropic plate problems. Some work has focused on the analytical solutions for the buckling and postbuckling response of curved unstiffened laminated panels (e.g., Refs. 5–7). Postbuckling test results for flat unstiffened graphite-epoxy plates loaded in axial compression are compared with analytical predictions in Ref. 8. Only limited data have been published (e.g., Refs. 9–11) that describe the postbuckling behavior and failure characteristics of stiffened composite panels loaded in axial compression. Postbuckling test results for flat stiffened graphite-epoxy panels loaded in axial compression are compared with analytical predictions in Ref. 10.

This paper presents the results of an experimental and analytical study of the postbuckling response and failure characteristics of selected curved stiffened graphite-epoxy panels loaded in axial compression. Results for flat and curved stiffened panels with 16-ply quasi-isotropic skins and four equally spaced I-shaped stiffeners are compared to determine the influence of panel curvature on postbuckling response. A relatively heavy stiffener design was selected for the panels so that the nonlinear response of the panels would be primarily due to the buckling of the skins. The paper also describes the influence of measured surface imperfections on the predicted postbuckling response of the panels. Analytical results from the STAGSC-1 (Structural Analysis of General Shells[12]) nonlinear general shell finite-element analysis computer code are compared with typical test results and the level of analytical modeling detail needed to represent accurately their postbuckling response is described. Stress distributions in the interface region between the panel skin and the stiffener attachment flange were determined analytically using the POSTOP computer code (Postbuckled Open-Stiffener Optimum Panels[13,14]) and typical results are presented.

Experiment

Test Specimens

The eight specimens tested in this investigation were designed and manufactured by the Lockheed-Georgia Company under NASA Contract NAS1-15949. The specimens were fabricated from commercially available unidirectional Thornel 300 graphite-fiber tapes preimpregnated with 450 K cure Narmco 5208 thermosetting epoxy resin.‡ Typical lamina

Presented as Paper 85-0768 at the AIAA/ASME/ASCE/AHS 26th Structures, Structural Dynamics, and Materials Conference, Orlando, FL, April 15–17; 1985; received Aug. 5, 1985; revision received Oct. 1, 1987.

*Aerospace Engineer, Structural Mechanics Branch, Structures and Dynamics Division. Member AIAA.

†Head, Structural Mechanics Branch, Structures and Dynamics Division. Associate Fellow AIAA.

‡Identification of commercial products and companies in this paper is used to describe adequately the test materials. The identification of these commercial products does not constitute endorsement, expressed or implied, of such products by the National Aeronautics and Space Administration or the publisher of this Journal.

properties for this graphite-epoxy system are 127.4 GPa (18,500 ksi) for the longitudinal Young's modulus, 13.0 GPa (1890 ksi) for the transverse Young's modulus, 6.4 GPa (930 ksi) for the shear modulus, 0.38 for the major Poisson's ratio, and 0.14 mm (0.0056 in.) for the nominal ply thickness. Each specimen had four equally spaced I-shaped stiffeners of the same design. Stiffener spacing was varied to determine the effect of skin postbuckling response on panel performance. Specimens had 16-ply quasi-isotropic skins, 216 cm panel radius, and either 10.2, 14.0, or 17.8 cm stiffener spacing. The panel lengths were selected so the initial buckling modes would have at least four longitudinal halfwaves.

The panel geometry and stiffener details are shown in Fig. 1. Panel length L, panel arc length or width W, panel chord length C, panel radius R, and stiffener spacing b are shown schematically in Fig. 1a; stiffener geometry is shown in Fig. 1b; and the details of the tapered stiffener attachment flange are shown in Fig. 1c. The stacking sequences for the panel skins, stiffener webs, and stiffener caps are $[\pm 45/0_2/\pm 45/90_2]_s$, $[0/\pm 45/\pm 45/0_2/\pm 45/0_2]_s$, and $[0/\pm 45/\pm 45/0_2/\pm 45/0_2/90/0_3/90_2/0_4/90_2/0_2]_s$, respectively. The panel length, panel width, panel radius, panel skin thickness, and stiffener spacing dimensions of all specimens are given in Table 1.

All specimens were cured in an autoclave using the resin manufacturer's recommended procedure. The stiffeners of all of the specimens were secondarily bonded to the skins with 395 K cure American Cyanamid FM-73 adhesive. Following cure, the specimens were ultrasonically inspected to establish specimen quality. No detectable defects were found in any specimen. The ends of each specimen were potted in an epoxy-resin material to prevent brooming of the graphite fibers during testing. The potting material was encased in 4.4 cm long steel frames for protection. The loaded curved ends of the specimens were machined flat and parallel to permit uniform axial compressive loading. The unstiffened side of each specimen was painted white to reflect light so a moire-fringe technique could be used to monitor the out-of-plane displacement pattern during testing.

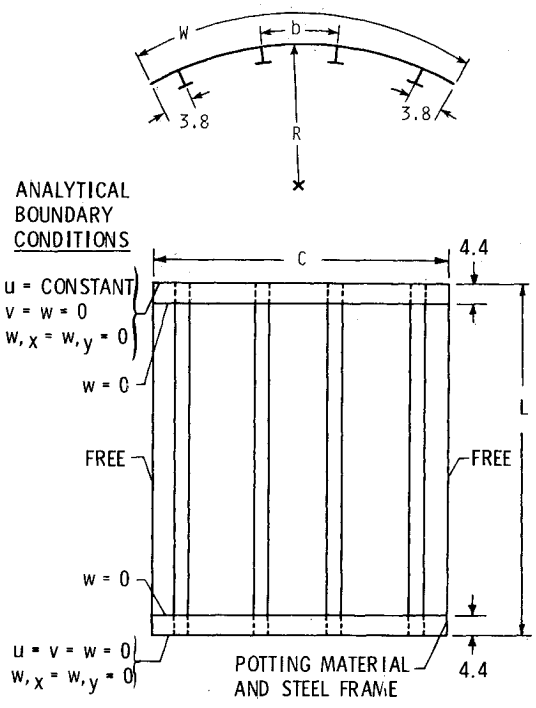

a) Panel geometry and analytical boundary conditions

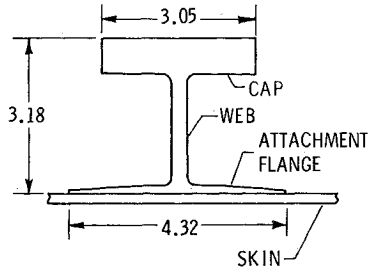

b) Stiffener geometry

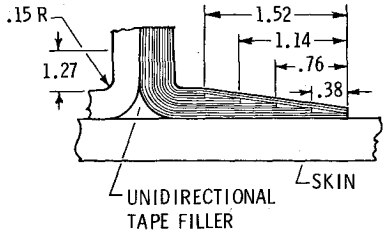

c) Stiffener attachment flange details

Fig. 1 Panel geometry, stiffener details and analytical boundary conditions (all dimensions in centimeters).

Initial Geometric Imperfection

Surveys to measure initial geometric imperfections of the panel skins were performed for several of the curved specimens using a contacting direct current differential transformer type of displacement probe in a traversing fixture. Elevation measurements were obtained along arcs of a specimen at 0.64 cm (0.25 in.) intervals along the length of the panel. Data were obtained dynamically as the probe was driven along each arc of a panel providing approximately 1000 samples/arc. The measured data represent the rise of the curved panel above a reference plane and are compared to the ideal rise of the panel based on a "best fit" radius of curvature. The difference between these two sets of values of the rise is referred to herein as the initial geometric imperfection. The method used to represent the geometric imperfections is described in Ref. 15.

Apparatus

Test specimens were loaded in axial compression using a 4.45 MN capacity hydraulic testing machine. The specimens were flat-end tested without lateral edge supports. Electrical resistance strain gages were used to monitor strains and direct-current differential transformers were used to monitor displacements at selected locations. All electrical signals and corresponding applied loads were recorded on magnetic tape at regular time intervals during the tests. Out-of-plane displacements were also monitored by the moire-fringe technique. Moire-fringe patterns were recorded photographically.

Tests

Eight curved specimens were tested to failure in static compression to determine their postbuckling behavior. Data for the flat specimens were obtained from Ref. 10. An exploratory study of the effect of repeated loading on postbuckling behavior was conducted using specimens C7 and C8. Each of these specimens was initially loaded beyond buckling until a noise from the specimen was heard. The specimen was unloaded and subsequently ultrasonically inspected for damage. This sequence was repeated several times with each subsequent loading exceeding the previous maximum load until panel failure occurred.

Table 1 Panel geometry and initial imperfection results

Specimen	Width, cm	Length, cm	Stiffener spacing, cm	Skin thickness, mm	Radius, cm		Initial imperfection $w_0(x, y)$		
					Nominal	Measured	$(w_0)_{max}/t$	$(w_0)_{mean}/t$	$(w_0)_{rms}/t$
Flat panels[10]									
F1	38.1	50.8	10.2	1.94	∞	—	—	—	—
F2	49.5	66.0	14.0	1.99	∞	—	—	—	—
F3	61.0	81.3	17.8	1.99	∞	—	—	—	—
Curved panels									
C1	38.1	50.8	10.2	2.06	216	167	0.41	0.06	0.12
C2	38.1	50.8	10.2	2.09	216	164	0.34	0.08	0.09
C3	49.5	66.0	14.0	2.09	216	—	—	—	—
C4	49.5	66.0	14.0	2.09	216	142	0.44	0.12	0.11
C5	61.0	81.3	17.8	2.19	216	—	—	—	—
C6	61.0	81.3	17.8	2.02	216	199	0.58	0.15	0.13
C7[a]	49.5	66.0	14.0	2.07	216	—	—	—	—
C8[a]	61.0	81.3	17.8	2.12	216	—	—	—	—

[a]Repeatedly loaded specimens.

Analysis

The analyses performed in this study included both linear buckling and nonlinear postbuckling calculations. Buckling calculations were performed to predict the initial buckling response of the specimens and to determine the level of analytical modeling detail required to predict accurately the postbuckling response of the specimens.

Stiffener Modeling

To determine the required level of analytical modeling detail, buckling solutions were determined using the efficient buckling analysis capability of the PASCO computer code (Panel Analysis and Sizing Code[16]). The buckling analysis used in PASCO is based on an orthotropic prismatic plate formulation and is considered to be very accurate. The PASCO buckling solutions indicate that the stiffener webs deform and that local bending occurs in the skin near the skinstiffener interface region in much the same manner as described in Ref. 10. Since PASCO does not have a nonlinear analysis capability, the STAGSC-1 nonlinear general shell finite-element analysis computer code[12] was used to perform the postbuckling analyses.

The PASCO buckling solutions indicate that the stiffener attachment flange affects the panel buckling load and corresponding mode shape by influencing the panel's effective stiffener spacing. Based on these solutions, it was assumed that an accurate model of the tapered attachment flange (see Fig. 1c) would be required for the STAGSC-1 postbuckling analysis. The STAGSC-1 postbuckling model was constructed to simulate the tapered flange and to minimize computational costs. To simulate the tapered flange, a stepped-flange model was developed with the appropriate stiffnesses for a PASCO model in the same manner as described in Ref. 10. Using PASCO, the buckling load for this model was calculated and used as a standard for comparison. Finally, an equivalent uniform-thickness flange finite-element model was developed for STAGSC-1 by adjusting the width $\bar{b}$ and the height $\bar{h}$ of the uniform-thickness flange to values of 17.8 and 1.4 mm, respectively, so that the STAGSC-1 model would have the same extensional stiffness and buckling solution as the PASCO stepped-flange model.

Postbuckling Analysis

The finite elements used in the STAGSC-1 model to predict the postbuckling response of the specimens are combined membrane and bending quadrilateral elements with midside nodes. The finite-element model consisted of six shell elements across the skin between the stiffeners and six shell elements per longitudinal half-wave of the buckling mode shape. The stiffener web was modeled by two shell elements between the skin and the stiffener cap and the same number of plate elements along the length as the skin. The stiffener cap was modeled as a discrete beam. The loading and boundary conditions used for the analysis were selected to be consistent with the test conditions. The loading condition corresponds to a uniform end shortening applied to one of the curved ends of the specimen. The boundary conditions used for the analyses are indicated in Fig. 1a. The effect of residual stresses due to curing was neglected in the analyses. The initial geometric imperfection shape was obtained from a half-wave sine Fourier expansion of the measured surface imperfection (see Ref. 15). Selection of the modal content of the measured initial geometric imperfections for use in the nonlinear analysis was based on the largest 20 values of the mean imperfection amplitudes.

In the past, the postbuckling response of a structure has been obtained analytically with STAGSC-1 by using the modified Newton-Raphson solution procedure, which increments a load parameter and solves for the corresponding solution vector. The problems associated with the use of a load parameter as an independent parameter are related to solution prediction beyond a limit point and to ill-conditioning of the tangent stiffness matrix in the neighborhood of a limit or bifurcation point. Recently, a method based on controlling an equilibrium path/arc length parameter instead of the load parameter has been introduced into the STAGSC-1 computer code. The arc length control procedure implemented in the STAGSC-1 computer code closely follows that proposed by Riks.[17]

Skinstiffener Interface Stress Analysis

The stress distributions in the interface region between the panel skin and the stiffener attachment flange were determined analytically using the POSTOP computer code (postbuckled open-stiffener optimum panels[13,14]). POSTOP is a preliminary design and analysis code for postbuckled panels with open section stiffeners. The buckled skin deformation mode modeled in POSTOP is based on Koiter's shear field theory[18] extended to orthotropic laminates. The mode shape depends on four parameters that are determined by the Rayleigh-Ritz procedure. The definition of the deformation mode is valid well into the postbuckling range of the panel skin response. The details of the interface stress analysis procedure incorporated in POSTOP are described in Ref. 19.

Results and Discussion

Test Results

Initial Buckling

Each specimen tested in this investigation buckled into a stiffened panel buckling mode in which both the stiffeners and

the skin deformed. Each specimen failed at an applied load greater than the experimental buckling load. The experimental prebuckling extensional stiffness, buckling load, failure load, and corresponding end shortenings and the predicted buckling load and corresponding end shortening are given in Table 2 for each specimen. Initial buckling was identified by monitoring data from back-to-back strain gages on the skin and from direct current differential transformers that measure out-of-plane displacements of the skins.

Postbuckling Response

Moire-fringe patterns representing out-of-plane displacements were used to identify the buckling mode shape of each specimen and to visually monitor the out-of-plane displacement patterns associated with the postbuckling response of the panel skins. The buckling mode of each specimen had one transverse half-wave between each stiffener and five longitudinal half-waves. A photograph of a typical moire-fringe pattern of the out-of-plane displacement pattern for specimen C1 with an applied load equal to 679 kN just before failure is shown in Fig. 2

End-shortening results for the flat and curved specimens are shown in Fig. 3 as a function of the applied compressive load. The end shortening u of each specimen is normalized by the specimen's analytical end shortening u_{cr} at buckling and the applied load P is normalized by the specimen's analytical buckling load P_{cr} given in Table 2. The analytical buckling solution is represented on Fig. 3 by the open circle. These results indicate that the load shortening response curves are similar for both flat and curved specimens. The reduction in extensional stiffness that occurs after buckling is illustrated by the change in slope of these load shortening response curves. The failure of each specimen is indicated in Fig. 3 by the filled symbols on the appropriate curve. The filled circles represent the failure of the flat specimens and the filled squares represent the failure of the curved specimens. Each specimen failed at an applied load greater than its analytically predicted buckling load.

Surface strain measurements from back-to-back strain gages at four locations on a typical specimen (i.e., C1) are shown in Fig. 4 as a function of applied load. The measured strain e is normalized by the analytical strain at buckling e_{cr} and the applied load P is normalized by the analytical buckling load P_{cr}. Data from longitudinal strain gages located at panel

Table 2 Results for flat and curved specimens

Specimen	EA, MN	Test results P_{cr}, kN	u_{cr}, cm	P_{fail}, kN	u_{fail}, cm	Analytical results P_{cr}, kN	u_{cr}, cm
Flat panels[10]							
F1	142	358	0.13	616	0.25	452	0.16
F2	148	214	0.09	518	0.25	243	0.11
F3	164	138	0.08	461	0.26	156	0.08
Curved panels							
C1	136	465	0.17	679	0.27	477	0.16
C2	142	438	0.19	662	0.26	477	0.16
C3	163	271	0.11	488	0.22	267	0.11
C4	147	281	0.13	463	0.26	267	0.11
C5	162	205	0.10	516	0.30	207	0.10
C6	164	186	0.09	482	0.28	207	0.10
C7 (1)[a]	150	270	0.12	404[b]			
(2)		251		438[b]			
(3)		247		460[b]			
(4)		248		492[b]			
(5)	144	240	0.11	529	0.25		
C8 (1)[a]	153	231	0.12	392[b]			
(2)		210		442[b]			
(3)	156	201	0.11	479	0.28		

[a]( ) load cycle. [b]Maximum load of cycle.

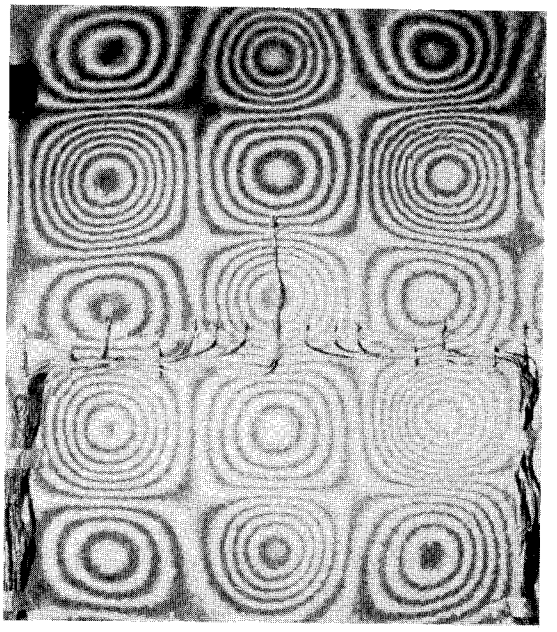

Fig. 2 Moire-fringe pattern of skin buckling mode just before failure for specimen C1 at 679 kN.

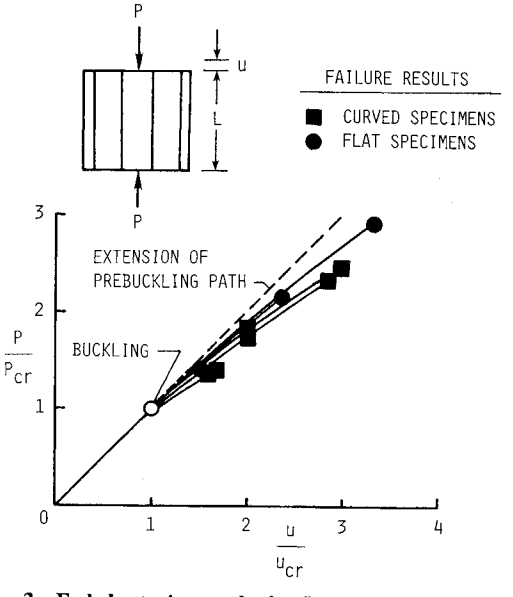

Fig. 3 End shortening results for flat and curved specimens.

midlength on the skin midway between the two inner stiffeners are shown in Fig. 4a. This pair of strain gages is located near a point of maximum out-of-plane displacement of the skin buckling mode and indicates that considerable bending can occur in the skin. Data from longitudinal strain gages located at panel midlength at the stiffener attachment flange of one of the inner stiffeners are shown in Fig. 4b. One of these gages is located on the stiffener attachment flange and the other on the panel skin. These gages indicate that relatively large strains can occur in the stiffener attachment flange. Data from two pair of back-to-back strain gages on the stiffener web near a quarter point of the panel length are shown in Fig. 4c. One pair of these gages (gages A and B in Fig. 4c) is oriented in the direction of the applied load and indicates that large membrane strains exist in the stiffener web. The other pair of these gages (gages C and D in Fig. 4c) is oriented normal to the panel skin (transverse to the direction of the applied load) and indicates that bending of the web about the loading axis

occurs after initial buckling. The results shown in Fig. 4 indicate that web buckling occurs at a load level of approximately 20% above the analytical panel buckling load (i.e., $1.2P_{cr}$).

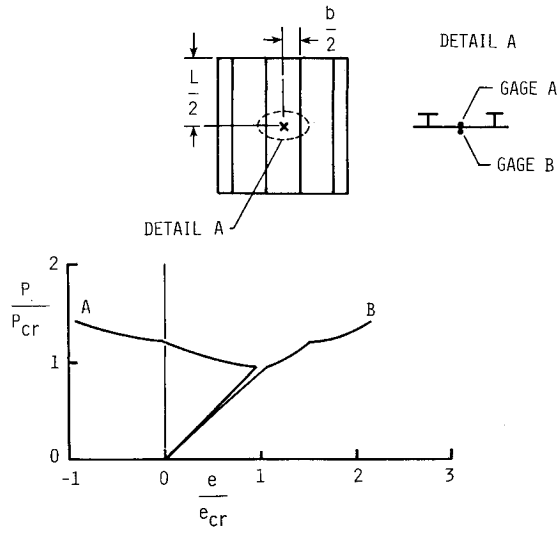

a) Skin surface strains midway between stiffeners

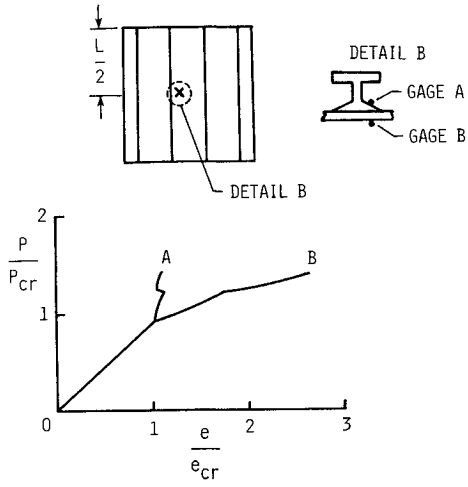

b) Surface strains on stiffener attachment flange

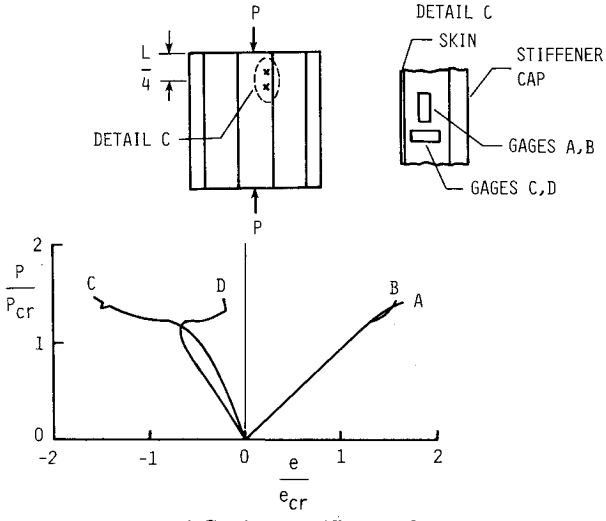

c) Strains on stiffener web

Fig. 4 Typical strain gage data for specimen C1.

Typical membrane strain distributions across the skin between stiffeners are shown in Fig. 5 for the curved specimens with 10.2, 14.0, and 17.8 cm stiffener spacings just before panel failure. The filled circles on the figure are the membrane strain e from back-to-back strain gage pairs located at a distance y from the left interior stiffener just before panel failure. The results in Fig. 5 indicate that increasing the stiffener spacing b of the panels decreases the magnitude of the membrane strains distributed across the panel. Membrane strain distributions for the curved specimens just before failure are similar to the membrane strain distributions given in Ref. 10 for the corresponding flat specimens. The membrane strains near the skinstiffener region are higher for the curved specimens than for the flat specimens.

The longitudinal membrane strain distribution is uniform for loads up to the buckling load. After buckling, the strain distribution has reduced membrane strains in the center of the skin bay and increased strains near the stiffeners at the edges of the skin bay. The differences in the magnitudes of the membrane strain in the center of the skin and the membrane strain at the stiffeners becomes larger as the applied load is increased above the buckling load. These higher strains at the stiffener attachment flanges contribute to a local failure in this skinstiffener interface region that causes panel failure.

Effect of the Panel Curvature

The effect of panel curvature on the postbuckling response of the specimens is shown in Fig. 6. The measured end shortening u normalized by the specimen length L is shown in the figure as a function of the applied load P normalized by the specimen prebuckling extensional stiffness EA. Experimental buckling results are indicated by the open symbols on the figure and panel failure is indicated by the filled symbols. The results in Fig. 6 indicate that each specimen has some postbuckling strength and that increasing the panel curvature increases both the initial buckling strains as expected from classical buckling theory and the failure strains. The effect of panel curvature combined with a large stiffener spacing resulted in a snap-through buckling phenomenon for the curved specimens with a 17.8 cm stiffener spacing.

Failure Characteristics

All specimens failed when the stiffeners separated from the skin in the interior of the specimens. A typical failed curved specimen (C1) is shown in Fig. 7. Buckling of the stiffener webs occurred prior to panel failure for the curved specimens with a 10.2 cm stiffener spacing. Stiffener web buckling in the curved specimens with 14.0 and 17.8 cm stiffener spacings was not detected.

The effect of repeatedly loading specimens C7 and C8 into the postbuckling range is indicated in Fig. 8. The out-of-plane displacement w measured near the center of the specimen normalized by the specimen skin thickness t is shown in Fig. 8 as a function of the applied load P normalized by the analytical buckling load P_{cr} for the initial and final loadings. Ultrasonic inspection after each load cycle detected local damage in the skinstiffener interface region. The results for the curved specimen with a 14.0 cm stiffener spacing shown in Fig. 8a indicate that the local damage accumulated from four previous loading cycles has lowered the buckling load by approximately 11% (also see Table 2). Apparently, the local damage changed the local stiffness characteristics of the panel enough to affect the buckling response. After buckling, the postbuckling response of the panel became asymptotic to that of the previous loading cycle. The results for the curved specimen with a 17.8 cm stiffener spacing shown in Fig. 8b indicate that the local damage accumulated from two previous loading cycles lowers the buckling load by approximately 13%. For specimen C8, the changes in the local stiffness of the panel apparently led to an abrupt change in the out-of-plane displacement pattern of the postbuckling response.

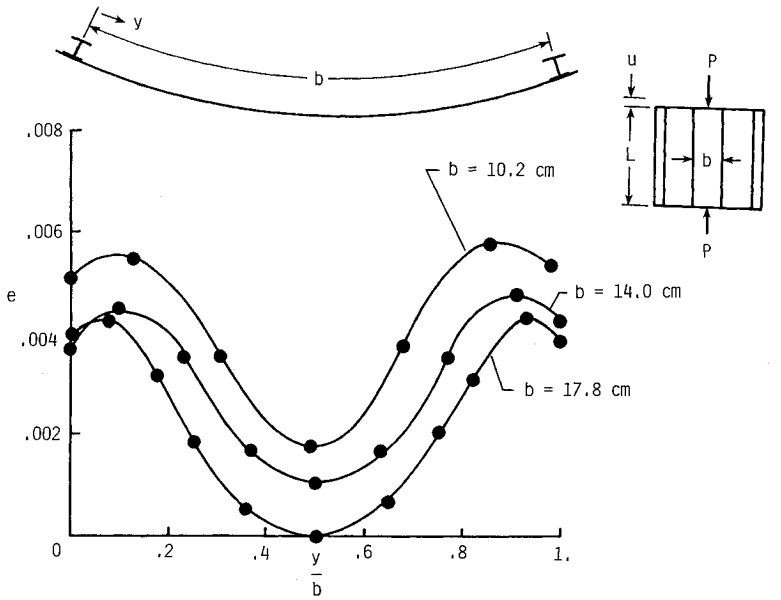

Fig. 5 Longitudinal membrane strain distributions for curved specimens just before failure.

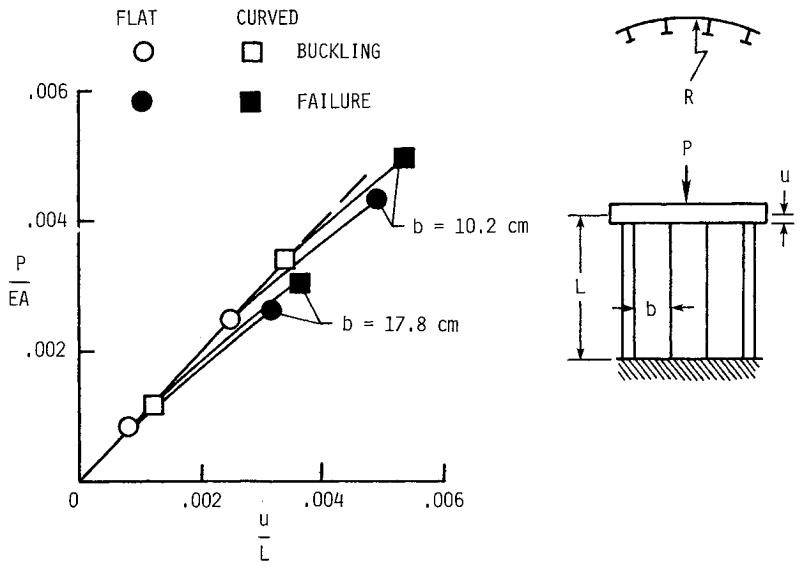

Fig. 6 End shortening results for 16-ply graphite-epoxy panels loaded in axial compression.

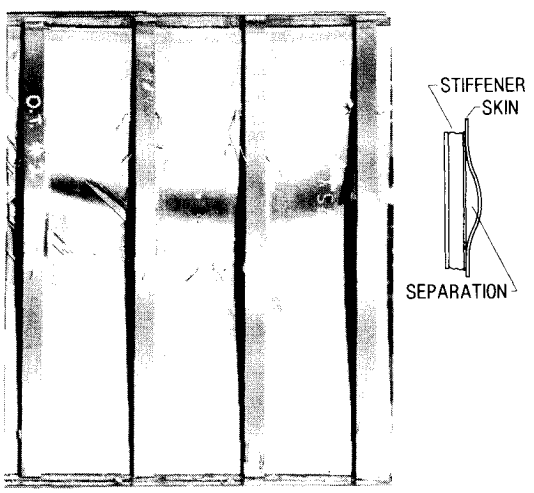

Fig. 7 Postbuckling failure mode of a stiffened graphite-epoxy curved compression panel with a 16-ply skin and 10.2 cm stiffener spacing.

Surface strain measurements from back-to-back strain gages at two locations on the skin midway between the two interior stiffeners of specimen C8 are shown in Fig. 9 as a function of the applied load normalized by the analytical buckling load. The panel was first loaded to 392 kN and unloaded when a noise was heard from the panel. The panel was then loaded to 442 kN in a five longitudinal half-wave mode and unloaded when additional noise was heard from the panel. While loading the panel to 479 kN on its third loading cycle, an abrupt change in the out-of-plane displacement pattern occurred at 427 kN. The change in mode shape is indicated on Fig. 9 by the change in the strain gage response at this load. Apparently, the local damage in the skinstiffener interface region was enough to change the postbuckling characteristics of the panel.

Analytical Results

Effect of Imperfections on Buckling

Buckling solutions were determined using the PASCO computer code[16] for various amplitudes of a bow-type imperfections to determine the influence of initial geometric imperfec-

tions on buckling. A negative bow-type imperfection causes additional compression in the skin. Increasing the amplitude of this imperfection has the effect of lowering the buckling load without changing the out-of-plane displacement pattern. A positive bow-type imperfection causes additional compression in the stiffener cap. Increasing the amplitude of this imperfection has the effect of raising the buckling load with a corresponding change in the out-of-plane displacement pattern. Initial imperfections affect the panel response by redistributing the applied load in the panel skin and the stiffener caps. Apparently, the initial geometric imperfection measured for specimen C1 causes additional compression in the panel skin, since the analytical buckling load exceeds the experimental values for the buckling load of both curved specimens with a 10.2 cm stiffener spacing.

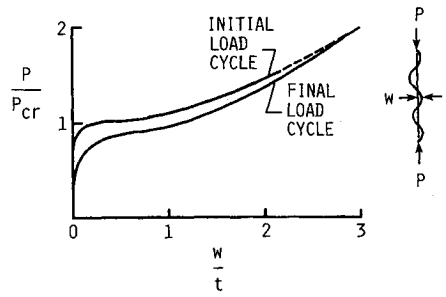

a) Specimen C7

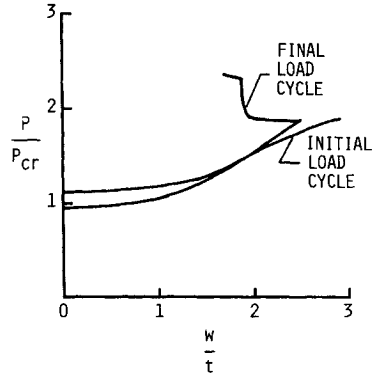

b) Specimen C8

Fig. 8 Out-of-plane displacements near panel midlength, midway between stiffeners for initial and final load cycles.

Postbuckling Response

Comparisons between test results and analytical results obtained with the STAGSC-1 computer code[13] are shown in Fig. 10 for a typical specimen (i.e., C1). End shortening u normalized by the analytical end shortening u_{cr} at buckling (Fig. 10a) and out-of-plane displacement w near a point of maximum displacement normalized by the specimen skin thickness t (Fig. 10b) are shown as functions of the applied load P normalized by the analytical buckling load P_{cr}. The open circles on the figure represent test data and the curves represent analytical data determined from STAGSC-1 by a nonlinear analysis. The filled circle on Fig. 10a represents the linear bifurcation buckling load of the specimen determined from STAGSC-1 by a buckling calculation. These experimental and analytical results correlate well up to the load where local failures influence the overall panel response. The finite-element model of the laminated panel assumes that the material system remains a linear elastic system throughout the analysis. The local failures, such as local delaminations or localized stiffener disbonding, which occur near the skin/stiffener interface region, can not be modeled analytically with STAGSC-1 at the present time. A progressive failure analysis capability that accounts for the local failure modes of composite structures would be required for such an analysis.

Contour plots of the out-of-plane displacements generated by the STAGSC-1 computer code at several values of the applied load are shown in Fig. 11. The out-of-plane displacements are normalized by the maximum value of the out-of-plane displacement w_{max} for each load step and the contour lines are at 5% increments of the maximum value. Prior to buckling, the imperfections cause the asymmetric deformation

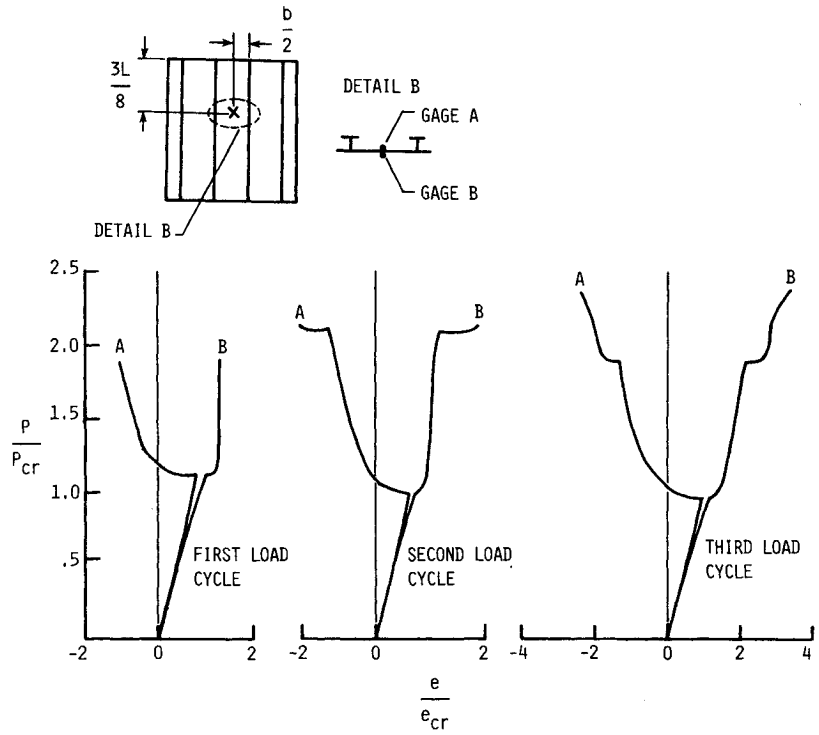

Fig. 9 Strain gage data for specimen C8 (skin surface strains midway between stiffeners above panel midlength).

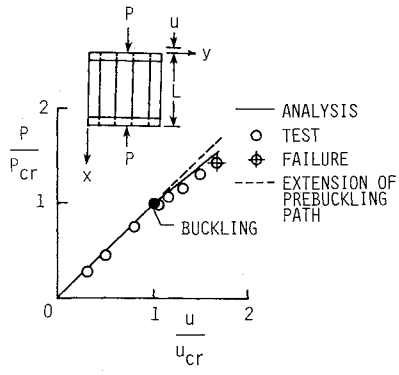

a) End shortening results

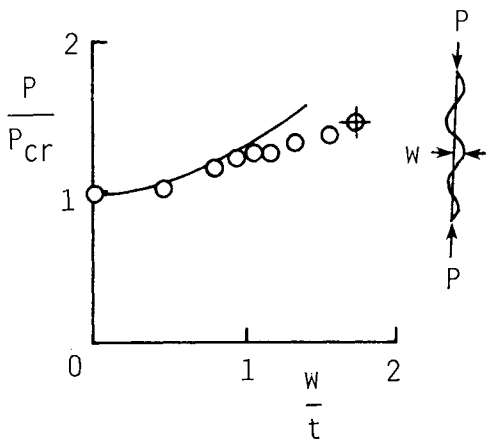

b) Out-of-plane displacement near a point of maximum buckling mode amplitude

Fig. 10 Comparison of experimental and analytical postbuckling response results for specimen C1.

pattern (see Fig. 11a). The pattern develops into a symmetric deformation pattern with five longitudinal halfwaves at a load level of approximately 1.1 P_{cr} (see Figs. 11b and 11c). Including the measured initial geometric imperfection in the postbuckling analysis allows the deformations to be predicted reasonably well. These analytically determined contour plots compare well qualitatively with the moire-fringe patterns observed during testing. The moire-fringe pattern of the skin buckling mode just before failure shown in Fig. 2 compares quite well with the predicted out-of-plane displacement pattern shown in Fig. 11d.

Skinstiffener Interface Stress Distributions

The failure of all specimens tested in the study and in the study reported in Ref. 10 is initiated by local skinstiffener separation. The high membrane strains in the vicinity of the stiffeners coupled with the large out-of-plane displacements are apparently sufficient to cause separation of the skin and the stiffeners. Using the POSTOP computer code,[13,14] the stress distributions in the adhesive interface layer between the skin and the stiffener attachment flange are determined for three values of skin loading. Stress distributions across the width of a stiffener attachment flange b_f are shown in Fig. 12 as a function of the distance y measured from the stiffener web midplane. The normal stress σ_z at a buckle crest is shown in Fig. 12a, the transverse shear stress τ_{yz} at a buckle crest in Fig. 12b, and the transverse shear stress τ_{xz} at a buckle node line in Fig. 12c. The shaded regions in the figure represent nominal design allowables for the interface adhesive material. The nominal design allowable values for the normal stress are 55 MPa (8 ksi) in tension and 207 MPa (30 ksi) in compression and the values for the transverse shear stresses are 62 MPa (9 ksi). Since POSTOP does not currently have a free-edge stress singularity analysis or a progressive failure analysis capability to relieve any severe stress concentrations, unusually large stresses for the interface material system may result from the analysis. The normal stress σ_z distribution shown in Fig. 12a and the transverse shear stress τ_{yz} distribution shown in Fig. 12b indicate that the maximum stresses occur near the stiffener web and exceed the nominal design allowables for the interface material for the values of skin loadings considered. As the longitudinal inplane loading in the skin is increased, the stresses that exceed the nominal design allowables extend toward the free edge of the stiffener attachment flange. The transverse shear stress τ_{xz} distribution shown in Fig. 12c indicates a severe free-edge stress gradient.

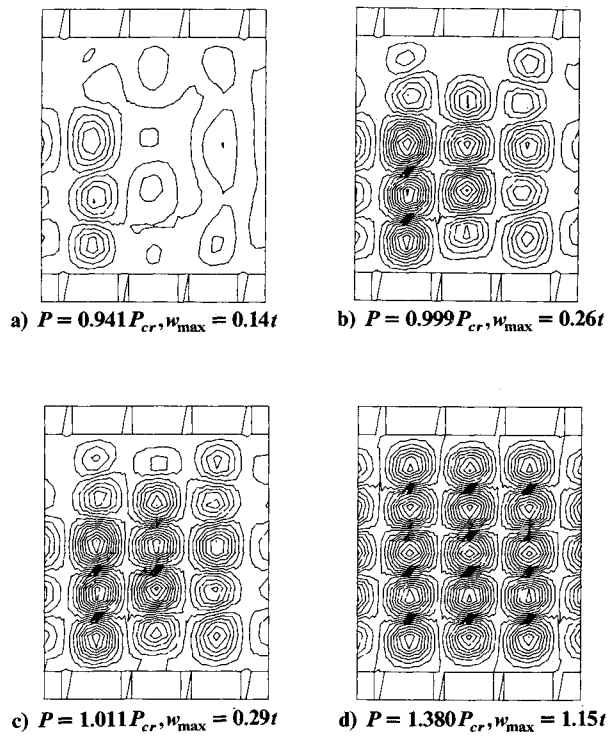

a) $P = 0.941P_{cr}, w_{max} = 0.14t$ b) $P = 0.999P_{cr}, w_{max} = 0.26t$

c) $P = 1.011P_{cr}, w_{max} = 0.29t$ d) $P = 1.380P_{cr}, w_{max} = 1.15t$

Fig. 11 Contour plots of out-of-plane displacement field of the analytically determined postbuckling solution for specimens C1.

Conclusions

An experimental and analytical investigation was conducted to study the postbuckling behavior of selected curved stiffened graphite-epoxy panels loaded in axial compression. Eight panels with a 216 cm radius of curvature and 16-ply quasi-isotropic skins were tested in this investigation. Each panel had four equally spaced I-shaped stiffeners. Panels with three different stiffener spacings were tested. Two of the panels were subjected to repeated loading beyond the buckling load to observe the effect of the growth of local damage on the postbuckling response prior to panel failure.

The buckling mode of all specimens was a stiffened panel buckling mode in which both the stiffeners and the skin deformed. Failure of all panels appeared to initiate in a skinstiffener interface region. The high membrane strains that exist at the stiffeners after skin buckling are apparently sufficient to cause a local skinstiffener separation that contributes to the overall panel failure. Local damage that occurred prior to panel failure changed the postbuckling response characteristics of the panels that were loaded repeatedly beyond buckling. Apparently, the local damage changes the panel stiffness enough to affect postbuckling response on subsequent loading cycles.

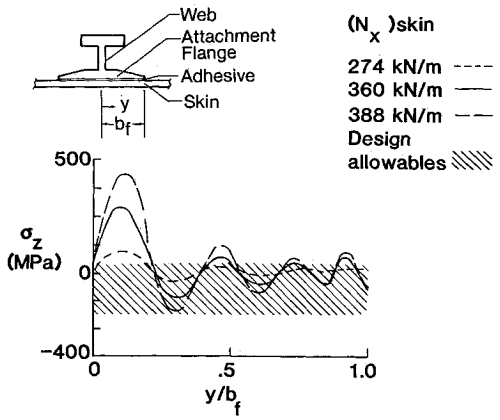

a) Normal stress σ_z at buckle crest

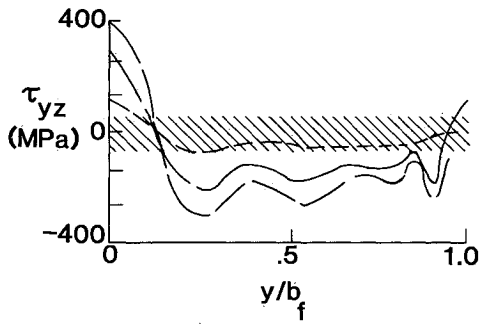

b) Transverse shear stress τ_{yz} at buckle crest

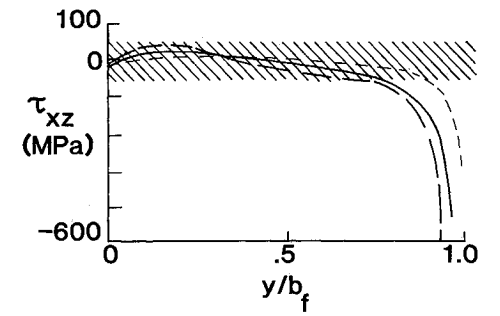

c) Transverse shear stress τ_{xz} at buckle node line

Fig. 12 Interface stress distributions across attachment flange for a specimen with 16-ply skin and 10.2 cm stiffener spacing.

Analytical results from the STAGSC-1 nonlinear general shell finite-element analysis computer code correlate well with typical postbuckling test results up to the load where local failures initiate. Since the analytical buckling mode had considerable deformation in the stiffener webs and attachment flanges, it was necessary to model these stiffener components with shell elements having the appropriate stiffnesses to obtain satisfactory correlation with the postbuckling test results. Measured initial geometric imperfections were used to model the panel skin geometry. Use of these measured imperfection data allowed the panel response to be predicted accurately until local damage occurred in the panel.

Analytical results from the POSTOP computer code indicate qualitatively that the stresses in the interface region between the skin and the stiffener attachment flange lead to local failures. These local failures apparently initiate in the interface region near the stiffener web and progress toward the free edge of the stiffener attachment flange to fail the panel.

References

[1]Turvey, G.J. and Wittrick, W.H., "The Large Deflection and Postbuckling Behaviour of Some Laminated Plates," *Aeronautical Quarterly*, Vol. 24, 1973, pp. 77–84.

[2]Harris, G.Z., "Buckling and Post-Buckling of Orthotropic Laminated Plates." AIAA Paper 75-813, May 1975.

[3]Harris, G.Z., "The Buckling and Post-Buckling Behaviour of Composite Plates Under Biaxial Loading," *International Journal of Mechanical Sciences*, Vol. 17, 1975, pp. 187–202.

[4]Banks, W.M., "The Post Buckling Behaviour of Composite Panels," *Proceedings of the* 1975 *International Conference on Composite Materials*, 1976, The Metallurgical Society of AIME, New York, Vol. 2, pp. 272–293.

[5]Khot, N.S., "Buckling and Postbuckling Behavior of Composite Cylindrical Shells Under Axial Compression," *AIAA Journal*, Vol. 8, 1970, pp. 229–235.

[6]Zhang, Y. and Matthews, F.L., "Postbuckling Behaviour of Cylindrically Curved Panels of Generally Layered Composite Materials with Small Initial Imperfections of Geometry," *Proceedings of the Second International Conference on Composite Structures, Composite Structures* 2, edited by I.H. Marshall, Applied Science Publishers, New York, 1983, pp. 428–441.

[7]Whitney, J.M., "Buckling of Anisotropic Laminated Cylindrical Plates," AIAA Paper 83-0979, May 1983.

[8]Starnes, J.H. Jr. and Rouse, M., "Postbuckling and Failure Characteristics of Selected Flat Rectangular Graphite-Epoxy Plates Loaded in Compression," AIAA Paper 81-0543, April 1981.

[9]Starnes, J.H. Jr., "Buckling and Postbuckling Research on Flat and Curved Composite Panels," *Selected NASA Research in Composite Materials and Structures*, NASA CP-2142, 1980, pp. 35–78.

[10]Starnes, J.H. Jr., Knight, N.F. Jr., and Rouse, M., "Postbuckling Behavior of Selected Flat Stiffened Graphite-Epoxy Panels Loaded in Compression," *AIAA Journal*, Vol. 23, Aug. 1985, pp. 1236–1246.

[11]Starnes, J.H. Jr., Dickson, J.N., and Rouse, M., "Postbuckling of Graphite-Epoxy Panels," *ACEE Composite Structures Technology: Review of Selected NASA Research on Composite Materials and Structures*, NASA CP-2321, 1984, pp. 137–160.

[12]Almroth, B.O., Brogan, F.A., and Stanley, G.M., "Structural Analysis of General Shells, Vol. II, User Instructions for STAGSC-1," Lockheed Palo Alto Research Laboratory, Palo Alto, CA, Rept. LMSC-D633873, Dec. 1982.

[13]Dickson, J.N. and Biggers, S.B., "POSTOP: Postbuckled Open-Stiffener Optimum Panels—Theory and Capability," NASA CR-172259, 1984.

[14]Biggers, S.B. and Dickson, J.N., "POSTOP: Postbuckled Open-Stiffener Optimum Panels—User's Manual," NASA CR-172260, 1984.

[15]Knight, N.F. Jr. and Starnes, J.H. Jr., "Postbuckling Behavior of Selected Curved Stiffened Graphite-Epoxy Panels Loaded in Axial Compression," AIAA Paper 85-0768-CP, April 1985.

[16]Anderson, M.S. and Stroud, W.J., "A General Panel Sizing Computer Code and Its Application to Composite Structural Panels," *AIAA Journal*, Vol. 17, Aug. 1979, pp. 892–897.

[17]Riks, E., "On the Numerical Solution of Snapping Problems in the Theory of Elastic Stability," Stanford University, Stanford, CA, Rept. SUDDAR 401, Aug. 1970.

[18]Koiter, W.T., "Het Schuifplooiveld by Grote Overschrydingen van de Knikspanning," National Luchvaart Laboratories, Amsterdam, Rept. S295, Nov. 1946 (in Dutch).

[19]Wang, J.T.S. and Biggers, S.B., "Skin/Stiffener Interface Stresses in Composite Stiffened Panels," NASA CR-172261, 1984.